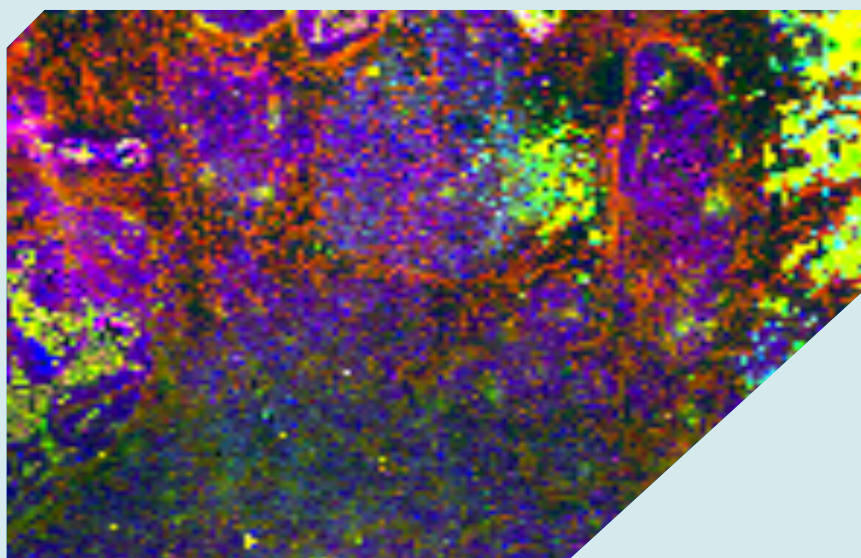
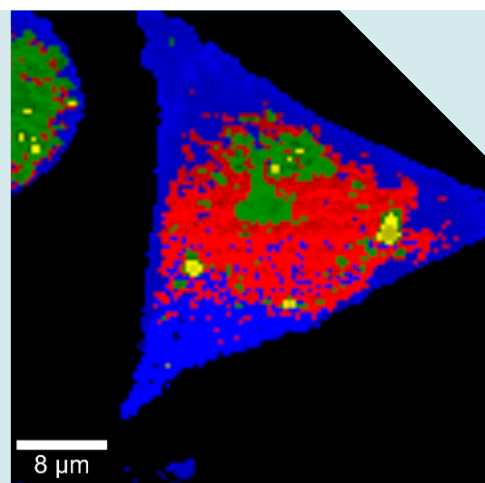
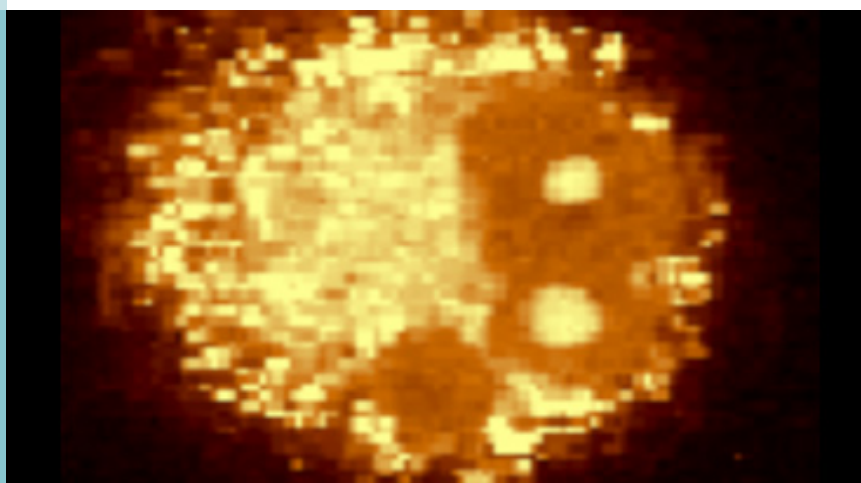
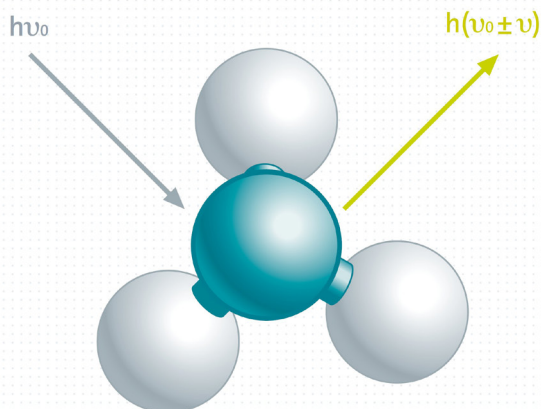


Advancing diagnostics and treatment with Raman imaging



Advancing diagnostics and treatment with Raman imaging

With confocal Raman imaging the molecules of a sample can be chemically identified and their distribution can be imaged three-dimensionally. These benefits are gaining more and more recognition in biological and medical research and confocal Raman microscopy (CRM) is becoming a more frequently used method for answering crucial questions in life sciences. CRM is used for measurements in liquids and live cell imaging, solid samples and soft tissues. Through various examples this application note describes possible uses of confocal Raman microscopy and correlative techniques.



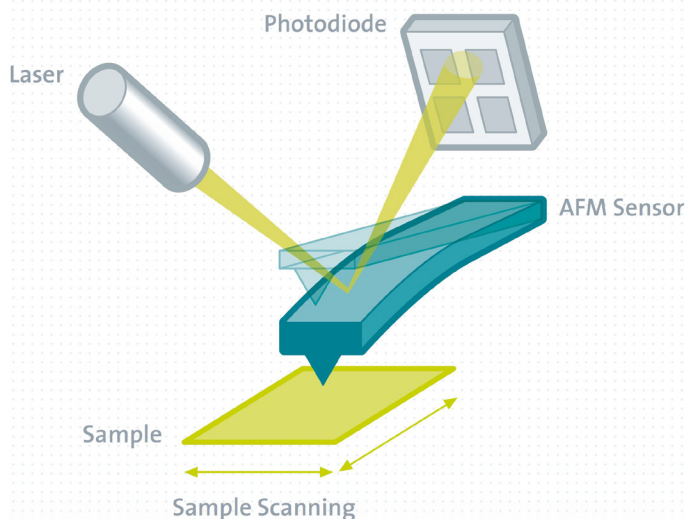
Working principles

Confocal Raman Imaging

The Raman effect is based on light interacting with the chemical bonds within a sample. This causes a specific energy shift in the backscattered light which appears in a unique Raman spectrum through which the molecular components of a sample can be detected.

The confocal Raman imaging technique combines Raman spectroscopy with a confocal microscope. This allows the spatial distribution of the chemical components within the sample to be imaged. High-resolution confocal Raman microscopes acquire a complete Raman spectrum at every image pixel and achieve a lateral resolution limited only by diffraction (circa $\lambda/2$ of the excitation wavelength).

A confocal microscope setup is furthermore characterized by an excellent depth resolution and facilitates the generation of 3D Raman images and depth profiles. Confocal Raman microscopy can be coupled with correlative microscopy techniques such as fluorescence microscopy, electron microscopy and atomic force microscopy.



Atomic Force Microscopy (AFM)

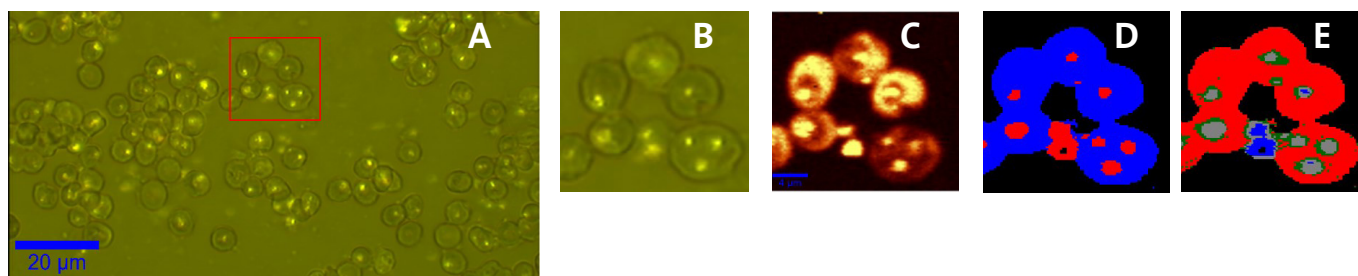
In AFM the sample is scanned under the tip using a piezo-driven scanning-stage and the topography is displayed as an image. AFM provides spatial information parallel and perpendicular to the surface with resolution in the nm range. In addition to topographic high-resolution information, local properties such as adhesion and stiffness can be investigated by analyzing the tip-sample interaction forces. In combination with confocal Raman imaging the topographic information can be linked to molecular information.

Raman microscopy in malaria diagnosis

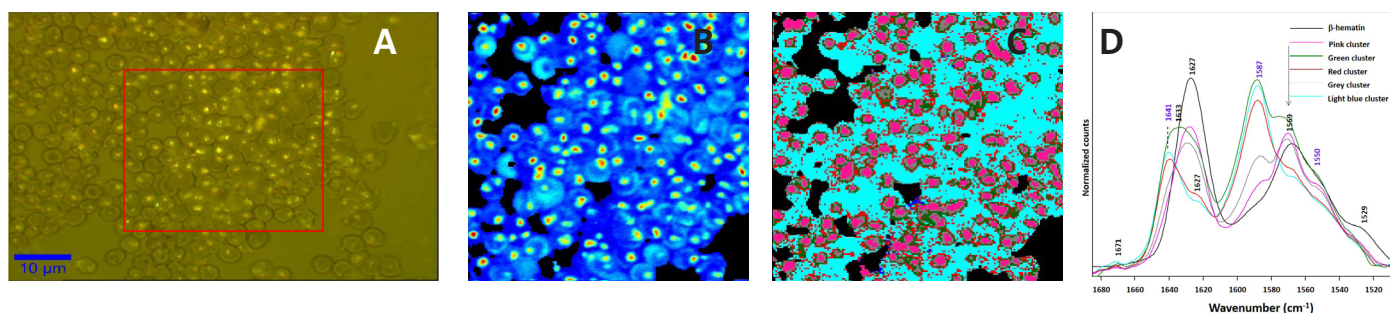
Raman microscopy can be applied as a rapid and accurate diagnostic tool for malaria. Malaria is caused by the parasite *Plasmodium* that infects human blood cells. In the blood cells it catabolizes large amounts of haemoglobin into an insoluble biomineral known as haemozoin (malaria pigment). In addition to serological antigen detection, this pigment is widely used for malaria diagnosis. A common microscopic method to detect haemozoin in malaria diagnosis is dark-field microscopy. Through darkfield microscopy haemozoin is presented as bright intracellular

lar spots. The combination of dark-field and Raman microscopy enables the comprehensive characterization of these spots and provides information about the stage of the disease. In the following study Raman spectroscopy was applied to detect and image small inclusions of haemozoin in *Plasmodium falciparum*-infected red blood cells. Therefore the confocal Raman microscope alpha300 R with a 532 nm Nd:YAG laser and a 60xNA=1.0 water immersion objective was used. The presence or absence of haemozoin was detected by the strong 1569 cm⁻¹ Raman band, which was used as a marker band for haemozoin. After data acquisition the spectral data was

further processed with WITec software. Cluster analysis was applied in order to facilitate the identification of haemozoin within the cells and to enable the classification of the different stages of the disease. Cluster analysis is suitable for the automatic identification of similar spectra and the classification of multi-spectrum data into a user-defined number of clusters. Thus color-coded, user-selected cluster images can be generated. The Raman results were compared with the dark-field micrographs in order to verify the analysis. For more details, please refer to the figure captions below.



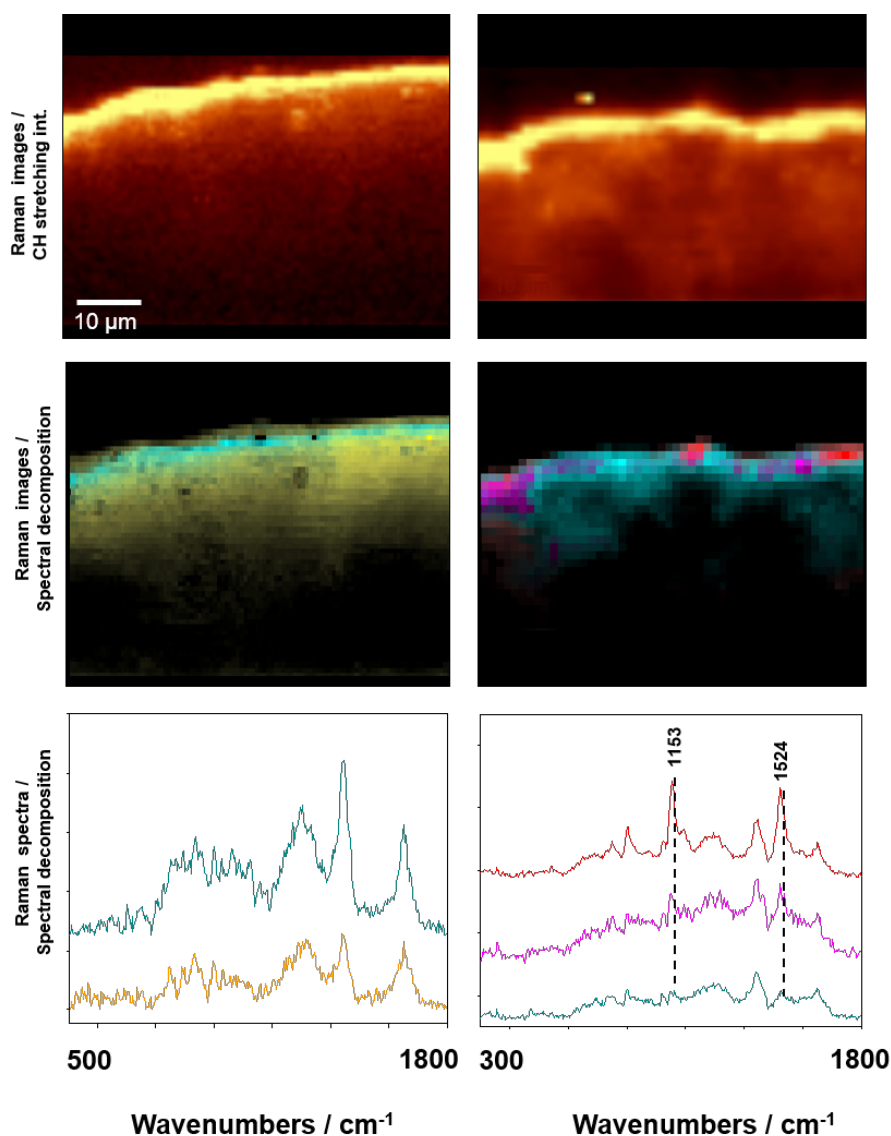
Verification of the analysis by comparison of dark-field and Raman microscopy (A) Visible micrograph showing the partial dark-field effect illuminating haemozoin deposits in several parasite infected cells. (B) Zoom-in of the red square in (A): The infected erythrocyte towards the bottom right corner is triply infected. (C) Chemical Raman map generated by integrating over the region between 1700 and 1500 cm⁻¹. The lighter color shows regions of higher counts. (D and E) Unsupervised Hierarchical Cluster Analysis (UHCA) map generated for the 1700–1500 cm⁻¹ range for 2 clusters (D) and for 5 clusters (E). The haemozoin particles can be clearly identified by Raman cluster analysis.



Identification of haemozoin in different stages of the disease (A) Visible partial dark-field micrograph of a thick film of malaria-infected cells showing the malaria pigment haemozoin as light intracellular dots (B) Chemical map of the 1569 cm⁻¹ Raman band of approximately the area bounded by the red square in (A). The yellow and red features depict the haemozoin deposits in the blood cells. (C) Cluster analysis performed using the range between 1700 cm⁻¹ and 1300 cm⁻¹ showing 5 clusters. The pink cluster correlates to the haemozoin deposits within late-stage infected blood cells. The green and grey clusters are a mixture of haemoglobin and haemozoin. The light blue cluster correlates well with haemoglobin within the cell while the red-sub-micron sized dots (300 nm) appear to be inclusions of haemozoin observed in cells of different infection stages. (D) Mean extracted spectra from a 5 cluster analysis showing the region between 1600 and 1500 cm⁻¹. The colors correspond to (C) Note the differences in the red and light blue spectra. The strong shoulder on the pink spectrum centered at 1569 cm⁻¹ indicates that the sub-micron-dots observed in (C) are from inclusions of haemozoin.

Depth profiles of human skin

In the following study the transdermal delivery of pharmaceutical agents was investigated with Raman depth profiles of human skin tissue. Skin penetration experiments were performed by applying *beta*-carotene to the skin biopsies. After incubation x-zRaman profiles of the intact full thickness skin biopsies were generated and spectral images were acquired using an alpha300 R microscope with a 50x 0.9 NA objective and a 785 nm excitation laser. Depth profiles were collected by employing the x-zscan mode starting at the bottom of the image. The spectral information in the images highlights the different components of the tissue and the presence of the agents. Raman images of untreated skin and diffusion patterns for *beta*-carotene are presented. For further information please refer to the figure caption.



Raman depth profile images of human skin. Images were collected using 785 nm excitation and a step size of 1 μm . (A) and (B) show Raman images of normal untreated skin (B) preprocessed using a spectral unmixing algorithm. The associated spectra plotted in (C) exhibit the typical protein characteristic peaks at 1650 – 1800 cm^{-1} . The Raman images (D) and (E) show depth profile images of skin treated with a *beta*-carotene formulation. The distribution of *beta*-carotene is plotted in red and magenta. The associated spectra plotted in (F) show the characteristic Resonance Raman bands of *beta*-carotene at 1524 and 1153 cm^{-1} .

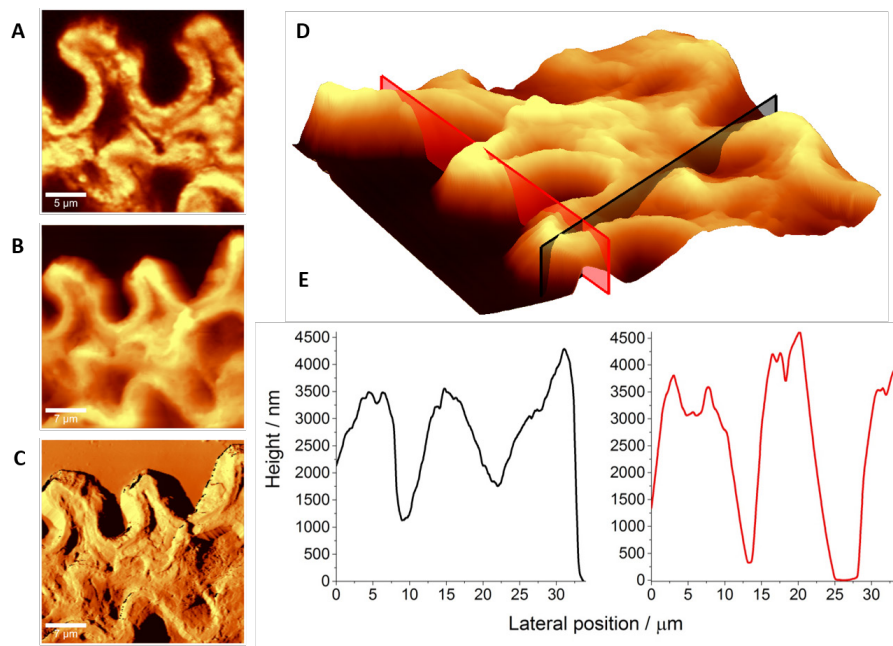
Imaging of vessels with combined Raman-AFM

Vessels consist of three main parts: tunica intima, media and adventitia. Changes to the vessel tissue structure and biochemical composition can indicate pathological alterations of the tissue, especially in endothelial cells. Those changes can be symptoms of vessel diseases e.g. diabetes, hypertension and atherosclerosis. Immunohistochemical (IHC) staining is a well-established method in pathology for analyzing the cellular compartments of a sample. While for

IHC staining the sample is treated with fluorescent dyes, Raman spectroscopy distinguishes specific tissue and cell constituents by integration of the appropriate Raman band. In many cases the information obtained with these two methods is the same. In the following study, an alpha300 RA fully integrated Raman-AFM microscope was used to investigate murine vessels. The Raman-AFM cross-section analyses of the vascular wall status are useful for monitoring ex vivo disease progression and the effects of treatment for diabetes, atherosclerosis and hypertension. While Raman spec-

troscopy provides specific biochemical information about the sample composition, AFM (Atomic Force Microscopy) detects the topography, structure and physical properties, e.g. stiffness and adhesion, of the samples surface. Thus combined Raman-AFM analyses are useful for the comprehensive characterization of the vessel status and both pathological and physiological conditions can be investigated and distinguished. In the following figure an exemplary Raman-AFM analysis of a vessel wall cross section is shown. For further information please refer to the figure caption.

Images of the vessel wall cross section: Raman distribution image of organic vessel specimens (A). AFM AC (intermittent or tapping mode) images of the vessel topography shown in (B) and the phase image shown in (C). The phase image reveals e.g. the tissue stiffness. The 3D topography imaging (D) was used to position the cross section (black and red lines). Through the cross-section profiles (E) the thickness of the vessel walls can be determined. Data acquired with an alpha300 RA fully integrated microscope, 100x/NA=0.9 air objective, 532 nm excitation laser, 10 mW laser power at the sample, integration time per Raman spectrum: 0.2 s. AFM topography image: AC (tapping) mode.

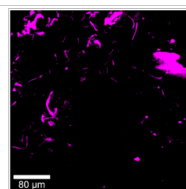
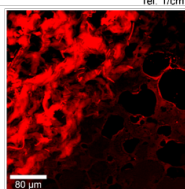
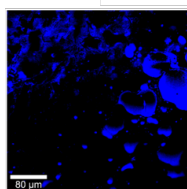
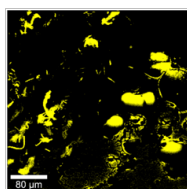
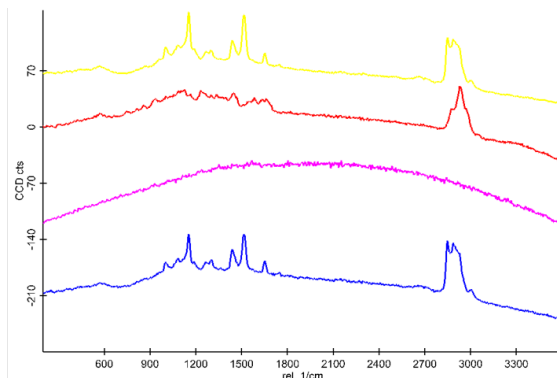
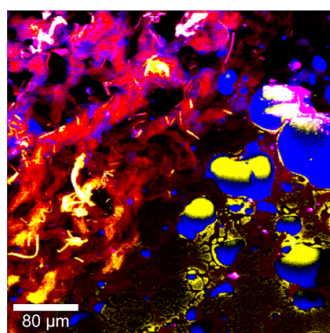


Comparison of noncancerous and cancerous tissue

Through confocal Raman imaging the general tissue composition as well as the appearance of tumor markers can be identified. Thus noncancerous and cancerous tissue can be distinguished and characterized without any external agent, staining or sample preparation

prior to the experiments. In this study noncancerous and cancerous human breast tissue of the same patient was examined with an alpha300 R confocal Raman microscope, a 50x objective, and a 532nm excitation laser with 10 mW laser power at the sample. The WITec Project Plus software was used for data acquisition and processing. The appearance of different

tissue components was determined through their unique Raman spectra and the noncancerous and cancerous tissues could be distinguished by the altered appearance of carotenoids, lipids and proteins. For further information please refer to the figure captions.

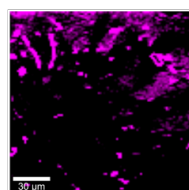
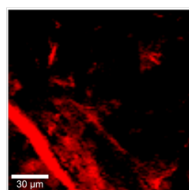
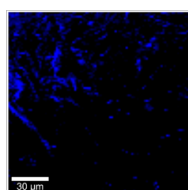
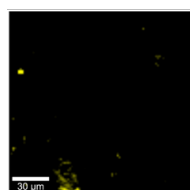
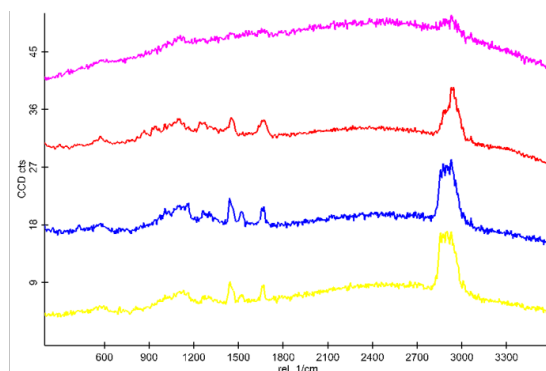
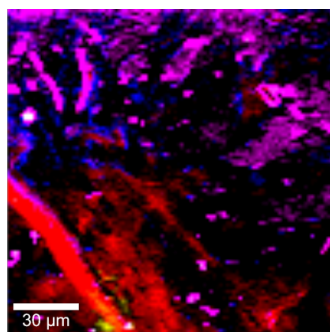


carotenoids

lipids

proteins

fluorescence



carotenoids

lipids

proteins

fluorescence

Breast tissue from the margin of the tumor mass:

Raman image ($350 \times 350 \text{ mm}^2$), integration time (per spectrum: 0.03 s), 1 accumulation; average spectra used for the basis analysis method. Colors of the spectra correspond to the colors of the different areas in the Raman image; images for the filters for spectral regions: carotenoids ($1490 - 1580 \text{ cm}^{-1}$), lipids ($2850 - 2950 \text{ cm}^{-1}$), proteins ($2900 - 3010 \text{ cm}^{-1}$) and fluorescence ($2200 - 2300 \text{ cm}^{-1}$). Please note that carotenoids are clearly detectable in the tissue.

Breast tissue from the tumor mass (carcinoma ductale G3 infiltrans mammae): Raman image ($150 \times 150 \text{ mm}^2$), integration time (per spectrum: 0.03 s), 1 accumulation; average spectra used for the basis analysis method, colors of the spectra correspond to the colors of the different areas in the Raman image; images for the filters for spectral regions: carotenoids ($1490 - 1580 \text{ cm}^{-1}$), lipids ($2850 - 2950 \text{ cm}^{-1}$), proteins ($2900 - 3010 \text{ cm}^{-1}$), and fluorescence ($2200 - 2300 \text{ cm}^{-1}$). Please note that the amount of detectable carotenoids is strongly reduced.

Images courtesy of Halina Abramczyk and Beata Brozek-Pluska, Lodz University of Technology, Institute of Applied Radiation Chemistry, Laboratory of Laser Molecular Spectroscopy, Wroblewskiego 15, 93-590 Lodz, Poland.